Journal of Materials Chemistry A

Accepted Manuscript

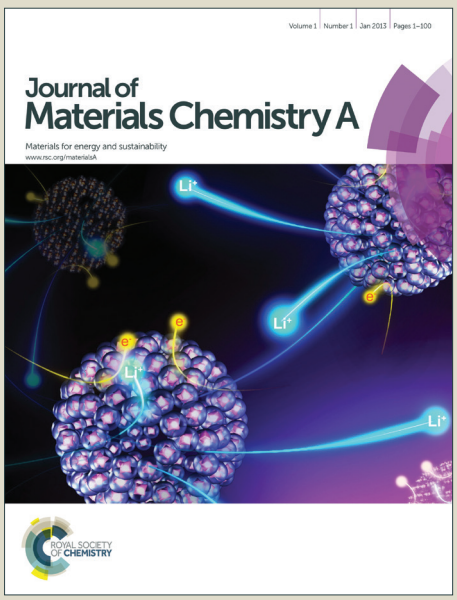

ROYAL SOCIETY OF CHEMISTRY

www.rsc.org/materialsA

Journal Name

RSCPublishing

ARTICLE

The effects of Ta_2O_5-ZnO films as cathodic buffer layers in inverted polymer solar cells

Cite this: DOI: 10.1039/xoxxoooooox

Received ooth January 2012,
Accepted ooth January 2012

DOI: 10.1039/xoxxoooooox

www.rsc.org/

Jo-Lin Lan[a], Sheng-Jye Cherng[a], Yi-Hsun Yang[a], Qifeng Zhang[a], Fumio S. Ohuchi[a], Samson A. Jenekhe[b] and Guozhong Cao[a]*

Ta_2O_5-ZnO composite films with varied composition were fabricated by sol-gel processing and applied as cathodic buffer layers (CBLs) for inverted polymer solar cells, and demonstrated enhanced power conversion efficiency with excellent stability. Physical and surface properties of Ta_2O_5-ZnO CBL films were examined by means of XPS, AFM, UV-Vis absorption spectra, and Goniometry. It is found that CBLs incorporated with Ta_2O_5 exerts two competing impacts on the solar cell performances. On one hand, the presence of Ta_2O_5 is likely to have induced more positive charges around Zn atom and form Ta-O-Zn bonding, and it can reduce the surface charge recombination between the bulk heterojunction (BHJ) active layer and cathodic buffer layer (CBL), and result in high power conversion efficiency; however, an excessive amount of Ta_2O_5 would block the pathways of charge transport and lead to a drastic reduction in the power conversation efficiency.

Introduction

Organic photovoltaic (OPV) devices have attracted a significant attention due to its acceptable energy conversion efficiency, potential to furnish low cost solar electricity, and capability to achieve portable application.[1–5] A conventional structure of OPVs (**Figure 1(a)**) consists of the bulk heterojunction (BHJ) active layer made by blending p-type polymer donor [6–8] with n-type fullerene acceptor [9,10] on the top of indium tin oxide (ITO) glass modified by the hole transporting layer (HTL), such as, poly(3,4 ethylenedioxylenethiophene):poly(styrene sulfonic acid) (PEDOT:PSS), molybdenum oxide (MoO_x), etc[11–14], and a low work function metal served as top electrode, typically aluminum, deposited on the top of active layer. The most widely studied polymer: fullerene system is based on a solution processed p-type Poly(3-hexylthiophene)(P3HT) polymer and an n-type [6,6]-phenyl-C_{61}-butyric acid methyl ester ($PC_{61}BM$) fullerene, and the highest efficiency of this system is around 5%.[3,10,15] By designing low band gap polymer material that can absorb boarder solar spectrum, controlling the microstructure of BHJ active layer to lengthen exciton diffusion length, and optimizing the device structure, efficiency as high as 10% was reported recently.[16]

In spite of dramatic improvement of power conversion efficiency and all the promising advantages, the conventional structure OPVs have a fatal weakness, i.e. the rapid performance degradation due to low work function top metal electrode, and unstable interface between ITO substrate and HTL,[17–19]; such a rapid performance degradation is unacceptable for any practical applications. Therefore, the inverted structure OPVs was proposed and studied to circumvent this drawback and demonstrated much improved performance stability.[20]

Comparing with the conventional structure OPVs, the charge flow path is opposite to that in the inverted one. **Figure 1(b)** depicts the inverted OPVs structure. A cathodic buffer layer (CBL), usually metal oxide, such as, ZnO, TiO_x, Nb_2O_5, Cs_2CO_3, or Al_2O_3[14,21–25], is deposited on ITO glass to reduce its work function in order to lower the barrier for electron transfer to ITO electrode. In addition, this kind of metal oxide needs to have the hole blocking and electron collecting ability to enhance the power conversion efficiency[26]. The top electrode is replaced by high work function metal, such as silver, to fulfill hole collection. The entire inverted structure is: ITO glass/metal oxide layer/ (BHJ) active layer / hole transporting layer (HTL)/Ag. The mechanism that the inverted structure OPVs have improved device stability is twofold: (1) the air sensitive, low work function top electrode (aluminum) is replaced with stable, high work function metal, either silver or gold, and (2) the interface between acidic PEDOT:PSS hole transporting layer and ITO glass is eliminated from the device.

Although inverted OPVs can improve the device stability, it suffers from relatively low power conversion efficiency, possibly due to the electron loss on the interface between BHJ active layer and the metal oxide layer, such as slow charge injection due to work function alignment, electron traps on CBL's surface defects.[27–30] For this reason, lot of studies focus on surface modification of metal oxide with self-assembled

monolayers, such as C_{60}-SAMs, saline, C_{60} molecules, and ethoxylated polyethylenimine (PEIE)[31–35] manipulating its morphology and surface energy, [23,36] and new material doping to enhance its electron collecting ability, such as, Al-doped ZnO, Ga-doped ZnO, zinc tin oxide, and $SrTiO_3$:ZnO. [37–41]

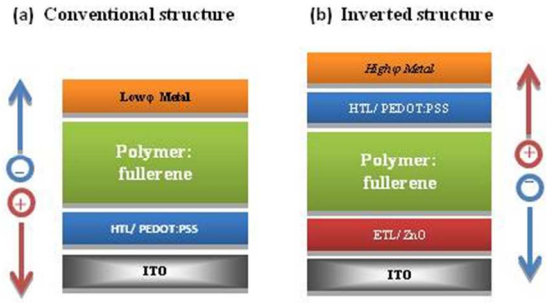

Figure 1. (a) Conventional structure (b) Inverted structure of OPVs and (c) the corresponding energy level diagram of the components of Inverted OPVs.

In this paper, we try to modify zinc oxide (ZnO) by introducing tantalum pentoixde (Ta_2O_5) as cathodic buffer layers (CBLs) for inverted structure OPVs. ZnO is n-type semiconductor with a wide band gap of 3.3eV and exhibits attractive features such as high electron mobility, good optical transmittance, and excellent stability.[42–45] Unfortunately, surface defect and the easy formation of oxygen vacancies at grain boundaries of ZnO often results in low conductivity of CBLs.[27–29,46,47] Tantalum pentoixde, on the other hand, is known for its high dielectric constant and index of refraction, and has found a variety of uses in electronics, such as tantalum capacitors for its high dielectric constant[48], antireflection coating for solar cells application due to its high refractive index and a low absorption coefficient (less than 10^3 cm^{-1}) for light,[49] and high-k dielectric for DRAM capacitor application.[50]

By applying Ta_2O_5-ZnO as cathodic buffer layer (CBL), the possible mechanism was proposed to explain the relation between CBL's composition, surface morphology, surface energy, and surface defect to photo-to-electrical energy conversion. PSEHTT/PC_{71}BM was also studied as BHJ active layer instead of P3HT/PC_{61}BM in inverted OPVs, and the long-term stability of unencapsulated inverted OPVs under ambient condition were also examined.

Experimental

***Materials*:** Regioregular Poly(3-hexylthiophene)(P3HT, 4002-E grade) was purchased from Rieke Metals, Inc. [6,6]-phenyl-C_{61}-butyric acid methyl ester (PC_{61}BM, 99.0% purity) was purchased from American Dye Source, Inc. Poly(3,4 ethylenedioxylenethiophene):poly(styrene sulfonic acid) (PEDOT:PSS, Clevios 4083) was purchased from H. C. Starck. poly[(4,4'-bis(3-(2-ethyl-hexyl)dithieno [3,2-b:'',3'-d]silole)-2,6-diyl-alt-(2,5-bis(3-(2-ethyl-hexyl)thiophen 2yl) thiazolo [5,4-d]thiazole)] (PSEHTT) and [6,6]-phenyl-C_{71}-butyric acid methyl ester (PC_{71}BM) were synthesized by Prof. Jenekhe's group. Zinc acetate ($Zn(CH_3COO)_2$, 98.0%), 2-methoxyethanol ($CH_3OCH_2CH_2OH$, 99.0%), monoethanolamine ($NH_2CH_2CH_2OH$–$2H_2O$, 99.0%), Tantalum(V) ethoxide ($Ta(OC_2H_5)_5$, 99.98%), Ethanol (CH_3CH_2OH, 99.5%, 200 proof absolute), Acetic acid (CH_3COOH, 99.7%) were purchased from Sigma-Aldrich. All the chemicals were used as received without further purification.ITO glass (10–15 Ω/sq) substrates were purchased from Colorado Concept Coatings LLC. Samples were prepared on ITO substrates (1.5*1.5 cm^2), which were cleaned prior to use by ultrasonic agitation in a detergent solution, acetone, and isopropyl alcohol, and then dried under nitrogen flow.

***Preparation of the Ta_2O_5:ZnO Cathodic Buffer Layers*:**

ZnO sol preparation

Zinc acetate dehydrate was first dissolved in a mixture of 2-methoxy ethanol and monoethanolamine at room temperature. The concentration of zinc acetate is 0.1 M and the molar ratio of monoethanolamine to zinc acetate was 1:1. The resulting solution was stirred using a magnetic stirrer at 60 °C for 2 h to yield a homogeneous, clear, and transparent sol.

$Ta(OR)_x$ sol preparation

Tantalum(V) ethoxide was first diulited in ethanol at room temperature, and then, acetic acid was added to form homogeneous, clear, and transparent sol. The final concentration of Tantalum(V) is 0.1M.

$Ta(OR)_x$-ZnO sol preparation

Both $Ta(OR)_x$ and ZnO sol's concentration are 0.1M, and simply mixed these two sols with molar ratio ($Ta(OR)_x$: ZnO =0:100, 6:84, 12:82, 18:82, 24:76, 30:70, 100,0) to form Ta_2O_5:ZnO sol.

The Ta_2O_5-ZnO sols were spin-coated after the prepared solution was aged at room temperature for one day in order to make it more glutinous. The sols were dropped onto ITO glass substrates, which were then spun twice at 3000 rpm for 30 s. After processing, the samples were immediately baked at 300°C for 10 min and subsequently annealed at 350°C for 20 min in air to convert to metal oxide. Throughout the device fabrication process, we fixed all the process parameters except Ta_2O_5-ZnO sol composition.

***Device Fabrication*:**

P3HT:PC_{61}BM solution preparation:

The chlorobenzene solution of P3HT:PCBM (1:0.8 by weight) containing (20 mg/mL) P3HT and (16 mg/mL) PCBM was stirred in glovebox at 60 °C overnight. The solution was allowed to cool to room temperature and then filtered through a 0.2 μm polytetrafluoroethylene (PTFE) filter.

P3HT:PC_{61}BM device:

First, the P3HT:PC_{61}BM blend solution was spin-coated onto the ITO substrates with the Ta_2O_5:ZnO buffer layer at 700 rpm for 30 s. Then the samples were baked at 225°C for 1 min to help self-organization of P3HT, as well as to drive away residual solvent and assist the polymer contact with the Ta_2O_5-ZnO cathodic buffer layer. Then, the diluted PEDOT:PSS solution was spin-coated onto the active layer to form the hole-transport layer. The films were then baked at 120°C for 10 min. A 100 nm thick Ag film was finally deposited under a vacuum of 2×10^{-6} Torr as the top electrode. The device structure of space-charge-limited-current (SCLC) measurement is the same only without PEDOT:PSS layer.

PHESTT:PC_{71}BM solution preparation:

PSEHTT/PC_{71}BM blend solutions with a composition of 1:2 ratio (wt:wt) was prepared by mixing 0.6 mL of the 6 mg/mL PSEHTT in 1,2-Dichlorobenzene with 0.12 mL of the 60 mg/mL PC_{71}BM in 1,2-Dichlorobenzene and 2.5% (vol/vol) processing additive of 1,8-octandithiol (ODT) in 1,2-Dichlorobenzene and stirred for 10 min at 100ºC on a hot plate.

PHESTT:PC_{71}BM device:

First, the PSEHTT/$PC_{71}BM$ blend solution was spin-coated onto the ITO substrates with the Ta_2O_5-ZnO buffer layer at 400 rpm for 40 s to form 60-70 nm active layer. Then the samples were vacuum-dried for 30 min. After that, 7.5nm MoO_3, and 120 nm Ag film were deposited under a vacuum of 2×10^{-6} Torr onto the active layer to form the hole-transport layer, and top electrode.

I-V Characterization:

The I–V characteristics of the solar cell were tested in a glovebox using a Keithley 2400 source measurement unit and an Oriel Xenon lamp (450 W) coupled with an AM1.5 filter. A silicon solar cell certificated by the national renewable energy laboratory (NREL) was used as a reference to calibrate the measurement conditions. The light intensity used in this study was 100 mW/cm^2.

Ta_2O_5-ZnO Buffer Layer Characterization : The surface morphologies of the specimens were obtained using AFM (Asylum Research MFP-3D Stand Alone AFM) operated in tapping mode. Optical transmittance spectra were recorded using a Thermo Fisher Scientific (EVO30 PC) UV–vis recording spectrophotometer over the wavelength range between 300 and 900 nm. XPS spectra and secondary electron cutoff were generated using a PHI Versaprobe system with an Al Kα X-ray source and a 100 μm beam size. The work function value was calibrated with pure gold foil (5.1 eV). Measurements were taken while the sample was under ultrahigh vacuum (10^{-10} Torr). The contact angle was measured by gonoimeter, and each sample was measured for four times in different area.

Results and discussion

Power conversion efficiency of the inverted OPVs with P3HT:$PC_{61}BM$ as BHJ layer

Figure 2 shows the I-V curves of the inverted OPVs with various Ta_2O_5-ZnO films as cathodic buffer layers (CBLs), and **Table 1** summarizes the I-V characteristics based on the results presented in **Figure 2**. Comparing with pure ZnO CBL, with a small amount of Ta_2O_5 (<18%) addition, the fill factor is found to increase from 0.61 to 0.67 monotonically with the increase of the amount of Ta_2O_5, while both short circuit current density and open circuit voltage remain unchanged at 0.63V and 9.7mA/cm^2, respectively. As a result, the overall power conversion efficiency increases from 3.7 % to a maximum of 4.12%. However, when the amount of Ta_2O_5 in the CBLs exceeds 24%, the power conversion efficiency turns to reduce rapidly, as a result of the sharp decrease of fill factor. For the OPVs with pure Ta_2O_5 as CBL, there is almost no detectable solar to electrical power conversion.

Such a change of power conversion efficiency with the increasing amount of Ta_2O_5 incorporated to the CBLs, first increase to a maximum and then decrease, indicates there are two competing and opposite mechanisms in play. A closer look reveals that the short circuit current density and open circuit voltage remain constant with <24% Ta_2O_5-ZnO films as CBLs in inverted OPVs, but, on the other hand, there are some differences in fill factor. The fill factor is known to be determined by series and shunt resistances of the solar cell device. The series resistance represents the overall series resistance and the shunt resistance is related to the recombination process in the device, respectively. As shown in **Table 1**, with a small amount of Ta_2O_5 (<18%) in CBLs, the series resistance stays at the same level, however the shunt resistance gradually increases from 0.67 to 3.3 k*ohm-cm^2. The increase in shunt resistance suggests that the charge recombination is reduced. While further increasing the amount of Ta_2O_5 to 24% or 30%, the increase in series resistance becomes predominant, resulting in low power conversion efficiency.

Table 1. I-V characteristics of inverted OPVs with various Ta_2O_5-ZnO CBLs. (BHJ active layer: P3HT:$PC_{61}BM$)

	Voc (V)	Jsc (mA/cm^2)	FF	Efficiency (%)	R_{sh} (kΩcm^2)	R_s (Ωcm^2)
Pure ZnO	0.636	9.49	0.613	3.70	0.67	8.72
6% Ta_2O_5	0.637	9.75	0.649	4.03	1	7.58
12% Ta_2O_5	0.634	9.73	0.661	4.08	5	7.20
18% Ta_2O_5	0.637	9.64	0.670	4.12	3.3	7.28
24% Ta_2O_5	0.631	9.75	0.616	3.79	1.67	10.07
30% Ta_2O_5	0.563	8.61	0.260	1.26	0.2	243.9
Pure Ta_2O_5	0.564	0.042	0.374	0.0009	11	125000

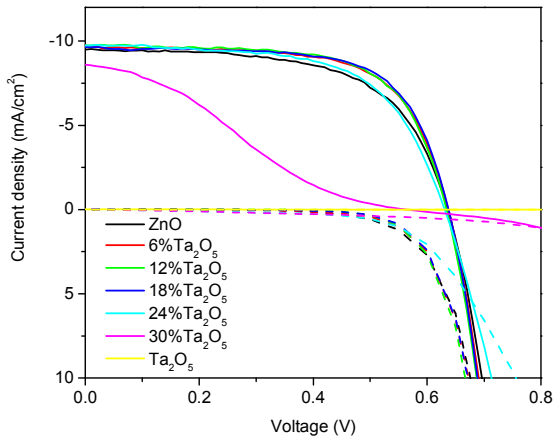

Figure 2. The I–V curve at 1sun and dark condition with various Ta_2O_5-ZnO films as the cathodic buffer layer. (BHJ active layer: P3HT:$PC_{61}BM$)

In order to understand the possible mechanisms by which the Ta_2O_5-ZnO films as CBLs affect power conversion efficiency (PCE) of the inverted OPVs, chemical and physical properties of the CBL were examined including transparency, morphology, surface energy, surface element composition, crystallinity, and electron mobility of Ta_2O_5-ZnO films.

Transparency of Ta_2O_5-ZnO films

Figure 3 compares the UV-Vis absorption spectra of various Ta_2O_5-ZnO thin films, and it is clear that the UV-Vis absorption spectra have no significant difference regardless the amount of Ta_2O_5. All Ta_2O_5-ZnO films have good optical transmittance in the visible region, with no appreciable antireflection effect with the incorporation of Ta_2O_5 in CBLs. It might be because the thickness of Ta_2O_5-ZnO film is so thin, only ~ 10 nm, and could be considered as totally transparent, so the introduction of various Ta_2O_5 amount in CBLs will no change its UV-Vis absorption spectra. Antireflection effect occurred when the thickness of Ta_2O_5 is up to 80 nm as reported in literature.[49] Almost identical UV-Vis absorption spectra of CBLs with varied chemical composition suggest that the transmittance of the CBLs is not a determining factor affecting the power conversion efficiency.

Surface Morphology and Surface Energy of Ta_2O_5-ZnO films

Figure 4 shows the AFM and contact angle images of Ta_2O_5-ZnO films on ITO glasses, and the root mean square (RMS) surface roughness and contact angle value are summarized in **Table 2**. It can be observed that the root mean square (RMS) value

decreases while a small amount of Ta_2O_5 blended into ZnO film (3.25nm (pure ZnO)→2.55nm (6% Ta_2O_5)), and gradually increases while increasing the Ta_2O_5 amount (2.55nm (6% Ta_2O_5)→3.05nm (30% Ta_2O_5)). Smoother surface (with lower surface roughness) could be good for serving as CBLs for the inverted OPVs as it might allow better contact of active polymer layer to the CBL.[23] However, it could not explain the fact there is a significant drop of PCE when the amount of Ta_2O_5 varied from 18 to 30% in CBLs since the surface morphology does not show much appreciable difference. The contact angle of the films in the range of 50~55° doesn't show detectable trend with varying the Ta_2O_5-ZnO composition, which means that the surface energy remains the same and unchanged regardless the addition of Ta_2O_5. All the films are slightly more hydrophilic compared with ITO glass.

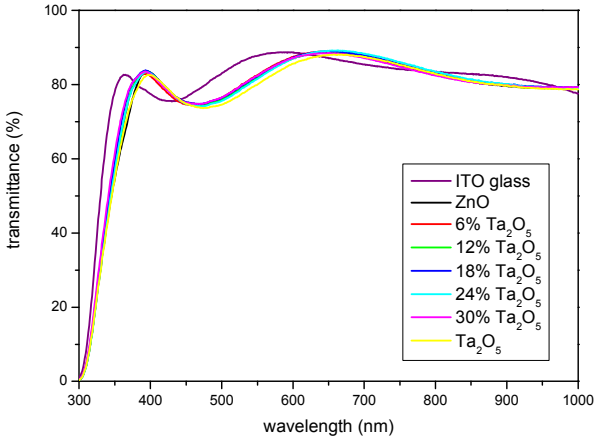

Figure 3. The UV–vis spectra of ITO glass and various Ta_2O_5-ZnO/ITO glass

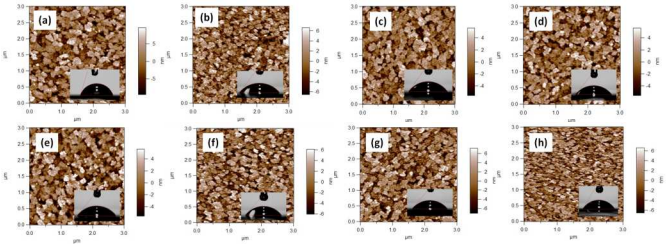

Figure 4. The surface morphology and contact angle of various Ta_2O_5-ZnO/ITO glasses. (a)ITO glass(b) ZnO (c)6% Ta_2O_5 (d)12% Ta_2O_5 (d)18% Ta_2O_5 (e)24% Ta_2O_5 (f)30% Ta_2O_5 (g)Ta_2O_5 on ITO glasses.

Work function and Surface Chemical Analysis of Ta_2O_5-ZnO films

The surface chemical analysis was carried out by means of X-ray photoelectron spectroscopy (XPS) (**Figure 5**). Both the Zn2$p_{3/2}$ and Ta4*f* data for each sample were scaled to the O1*s* emission intensity and shifted such that the O1*s* peaks have the same binding energy as 531 eV (this was necessary to account for charge neutralization plus some surface contamination that suppressed the intensities of the peaks during transfer to the XPS system). The Ta4$f_{7/2}$ and Zn2$p_{3/2}$ spectrum from the surfaces of the CBLs, their peaks are assigned as 26.35 and 1022.175eV which represents Ta_2O_5 and ZnO [51]. The intensity of Zn2$p_{3/2}$ decreased along with the addition of Ta_2O_5 whereas the intensity of Ta4*f* is increased while Ta_2O_5 concentration increased. As **Table 2** is shown, the peaks of Zn2$p_{3/2}$ shift to higher binding energy in the presence of Ta_2O_5, and it suggest that Zn^{2+} cation may be transformed to $Zn^{(2+\delta)+}$ and this transfer could be accounted for positively charged Ta^{5+}. When the concentration of Ta_2O_5 increased, Zn2$p_{3/2}$ peaks shift to higher binding energy; it can be proposed that Ta_2O_5-ZnO films do not only form as physical mixture with two distinct Ta_2O_5 and ZnO phases, but form chemical bond such as Ta-O-Zn in the system. If we correlate the XPS results with PCE data, it can be proposed that more positive charge around Zn might benefit the electron transfer from BHJ layer to CBLs or lower the possibility of electron recombination occurred on the interface between BHJ layer and CBLs.

Table 2. The root mean square (RMS) of surface roughness, contact angle, work function, XPS Zn 2$p_{3/2}$ peaks position difference with pure ZnO. (based on Zn2$p_{3/2}$=1022.175 eV) and electron mobility and electron mobility of various Ta_2O_5-ZnO/ITO glasses

	Roughness (nm)	Contact angle (°)	Work function (eV)	Δ binding energy (10^{-3}eV)	Electron mobility (cm^2/Vs)
ITO glass	4.42	71	-4.8	-	-
ZnO	3.25	52	-4.9	0	1.49E-05
6% Ta_2O_5	2.55	54	-4.69	63.6	1.67E-05
12% Ta_2O_5	2.63	54	-4.82	154.5	3.3E-05
18% Ta_2O_5	2.87	53.5	-4.91	295.3	2.3E-05
24% Ta_2O_5	3.05	55	-5.03	356.6	4.4E-06
30% Ta_2O_5	3.05	53	-4.94	388.4	1.1E-07
Ta_2O_5	3.36	60	-5.04	-	-

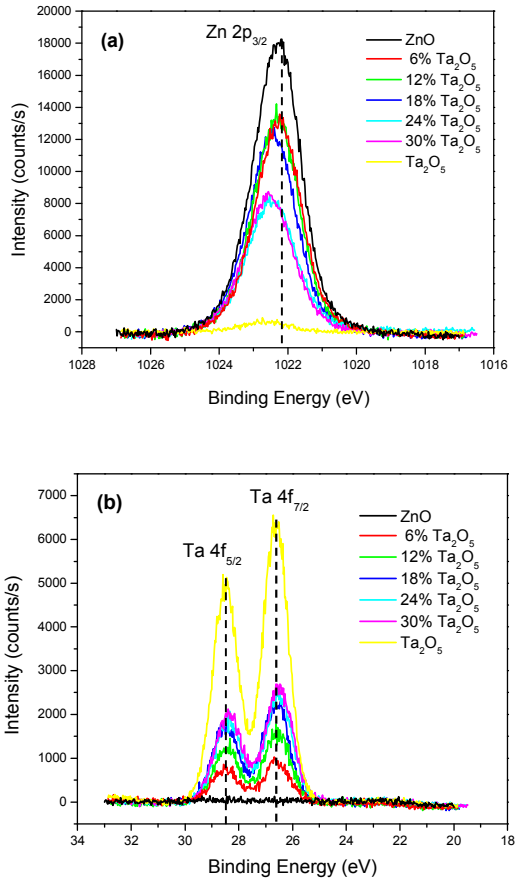

Figure 5. XPS results of various Ta_2O_5-ZnO/ITO glasses. Core levels of (a) Zn2$p_{3/2}$.(b) Ta 4f.

The work function was calculated using the X-ray photoelectron spectroscopy (XPS) secondary electron cut off region, and it was shown in **Table 2**. The work function of Ta_2O_5-ZnO film fluctuated with the chemical composition, first increased with Ta_2O_5 were added from -4.9 eV for pure ZnO film to -4.69 eV (6%Ta_2O_5-ZnO), and gradually decreased with more Ta_2O_5 was added. The high work function is favorable to electron transfer from BHJ active layer to CBLs in the inverted polymer solar cell application[35], however, the results obtained in the present investigation fell within the experimental error and demonstrated no direct relationship with the variation of power conversion efficiency. It definitely could not explain the fact that a significant drop of PCE in inverted OPVs with 24 and 30% Ta_2O_5-ZnO films used as CBLs.

Electron Mobility and Crystallinity of Ta_2O_5-ZnO films

The electron mobility can be determined by fitting the dark J–V curves for single carrier devices with space-charge-limited-current (SCLC) model[52]. The electron-only devices structure was ITO/Ta_2O_5-ZnO/P3HT:PCBM/Al fabricated to evaluate the electron mobility of Ta_2O_5-ZnO film by the charge transfer model of SCLC. The current is given by:

$$J= 9/8\times\varepsilon_0\times\varepsilon_r\times\mu_e\times V^2/D^3$$

where ε_0 is the permittivity of free space, ε_r is the relative permittivity of PCBM, μ_e is the electron mobility, and D is the thickness of active layer. From **Table 2**, comparing with pure ZnO device (1.49×10^{-5} $cm^2V^{-1}s^{-1}$), the electron mobility of <18% Ta_2O_5-ZnO devices keep in the same level as pure ZnO (~10^{-5} $m^2V^{-1}s^{-1}$). While continued increasing Ta_2O_5 adding amount, the electron mobility begin to drop drastically (~10^{-7} $m^2V^{-1}s^{-1}$), which can correlate with the poor power conversion efficiency with 24% and 30%Ta_2O_5-ZnO films as CBLs.

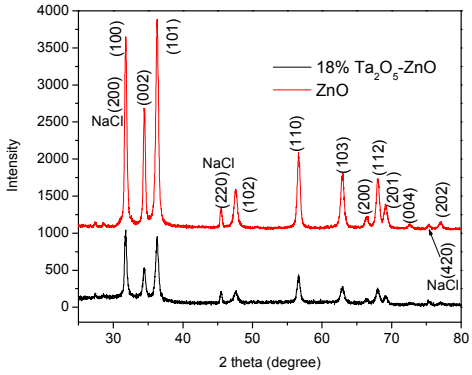

Figure 6. XRD results of 18%Ta_2O_5-ZnO and ZnO film. Noted that NaCl was added to the samples for XRD analyses and used as the reference to verify and confirm any possible change of lattice constants as a result of possible incorporation of Ta ions into ZnO crystals.

Moreover, the crystallinity of 18% Ta_2O_5-ZnO and pure ZnO films were examined by XRD, and the results were shown in **Figure 6**. NaCl was introduced by adding a drop of NaCl aqueous solution to the XRD samples and followed with crystallization at ambient environment and used to detect any possible instrumental shift of the XRD peak positions. From **Figure 6**, there is no signature peak represents Ta_2O_5, which means that Ta_2O_5 phase cannot be detected by XRD and more likely to form the amorphous phase. There existed no shift of any ZnO XRD peaks in low and high diffraction angles; this result is a clear indication that there is no change of lattice constant in ZnO crystals that further indicates that there is no incorporation of Ta ions into ZnO lattice. Moreover, the crystal size of these two films calculated by Scherrer equation are both 4.1nm. It is very reasonable considering the fact that Zn^{2+} has a coordination number of 4 with an ionic radius of 60 pm, whereas Ta^{5+} typically has a coordination number of 6 with an ionic radius of 65 pm [53]. However, its ionic radius is more likely to be <35 pm when subjected to a coordination number of 4 and, thus, it is very unlikely that Ta^{5+} would enter the ZnO crystal lattice. Moreover, the intensity of ZnO peak enormously reduced while Ta_2O_5 was present, which suggests that part of ZnO may also become amorphous. Recalling the XPS results presented and discussed earlier in this paper, we have demonstrated that there unambiguously exist Ta-O-Zn chemical bonds. The most reasonable explanation is that a fraction of ZnO formed an amorphous phase with Ta_2O_5 added to the film. Although it is not able to determine the chemical composition and the volume fraction of such amorphous phase, the amount of amorphous is likely to increase with an increased Ta_2O_5 added to the film. The presence of amorphous phase and/or the small amount of crystallinity ZnO will affect the electron transfer through CBLs, and result in low electron mobility, high series resistance and small fill factor. When the amount of Ta_2O_5 in CBLs reached a certain concentration, the amount of ZnO-Ta_2O_5 amorphous phase researched such a volume fraction that forms a uncontinuous network with ZnO crystals embedded and separated by such ZnO-Ta_2O_5 amorphous phase. Consequently the electron transfer through ZnO percolated network is restricted , resulting in a drastic reduction in fill factor and power conversion efficiency. When Ta_2O_5 is used as a CBL, there is no detectable solar-to-electrical power conversion. It should be noted that this result is different from what reported in an earlier paper [54]; where an inverted solar cell with Nb_2O_5 film as CBL did show ~3% power conversion efficiency. Although there is no clear explanation for such a discrepancy, Nb_2O_5 film (made with one spin-coating layer) reported in [54] was presumably much thinner, half of the thickness of Ta_2O_5 film (two spin-coating layers) investigated in this study, while tunneling conduction decreases exponentially with an increased thickness. In our previous work, the use of two spin-coating layers of Nb_2O_5 resulted in zero efficiency to the solar cell,[54] being well consistent with the Ta_2O_5 results presented here.

Furthermore, the improvement in fill factor might also be relative to the employment of different materials in CBLs and the change of film's surface chemistry[37–41]. It was reported that ZnO grain defects play an important role in decreasing the electrical conductivity. There are numbers of studies focus on the low conductivity of thin ZnO layers in OPVs, and it results from the presence of adsorbed oxygen at its grain boundaries. The adsorbed Oxygen can serve as an electron trap at these boundaries and therefore reduce the conductivity of these layers.[26,30,55] Therefore, both pure ZnO and 12% Ta_2O_5-ZnO films were annealing under oxygen or nitrogen atmosphere to simulate oxygen-rich or oxygen-barren in surface grain boundaries, and the results are shown in **Table 3** and **Figure 7**.

Table 3. I-V characteristics of inverted OPVs with various Ta_2O_5-ZnO CBLs. (Annealing under N_2 or O_2 atmosphere)

CBLs	Annealing atmosphere	Voc (V)	Jsc (mA/cm^2)	FF	Efficiency (%)
ZnO	N_2	0.63	9.99	0.61	3.82
	O_2	0.62	9.73	0.587	3.55
12% Ta_2O_5-ZnO	N_2	0.63	10.05	0.64	4.08
	O_2	0.64	9.99	0.64	4.06

It is found that, comparing processing under O_2 environment, the power conversion efficiency of the inverted OPVs with pure ZnO as CBLs was improved if it was annealed under N_2 atmosphere, which can be explained that the oxygen adsorbed in ZnO's grain

boundaries can be removed if we apply the N_2 atmosphere to process our CBLs. However, for the inverted OPVs with 12%Ta_2O_5-ZnO films as CBLs, the power conversion efficiency keeps the same as annealing in either O_2 or N_2 atmosphere. Although the exact mechanism to explain such insensitivity of Ta_2O_5-ZnO CBLs to O_2 and N_2 annealing is not known, the observation is likely to suggest that ZnO's surface grain boundaries, oxygen trapping sites, are somehow covered by Ta_2O_5 phase, or Ta_2O_5-ZnO becomes composite has less surface grain boundaries to adsorb oxygen molecules. Ta_2O_5 is known for its high dielectric constant and it is also proposed that high dielectric constant material would favor the effective charge transfer in PSCs.[40,47] Applying high dielectric constant material as CBLs might form an spontaneous polarization to create an internal electric field while PSCs operation and reduce the electron recombination possibility[40], which can also contribute to power conversion efficiency enhancement.

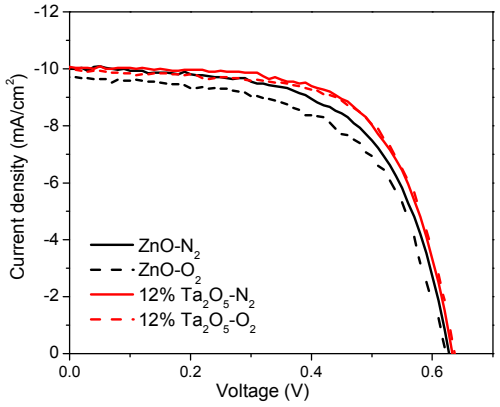

Figure 7. The I–V curve at 1sun with ZnO or 12%Ta_2O_5-ZnO films as the cathodic buffer layer.(Annealing under N_2 or O_2 atmosphere)

Table 4. I-V characteristics of inverted OPVs with various Ta_2O_5-ZnO CBLs. (BHJ active layer: PSEHTT:$PC_{71}BM$)

PSEHTT:PCBM	Voc (V)	Jsc (mA/cm²)	FF	Efficiency (%)
Pure ZnO	0.67	12.04	0.656	5.29
6% Ta_2O_5	0.67	12.17	0.675	5.51
12% Ta_2O_5	0.68	12.07	0.689	5.61
18% Ta_2O_5	0.67	12.36	0.667	5.57
24% Ta_2O_5	0.68	10.77	0.171	1.25
30% Ta_2O_5	0.77	0.05	0.482	0.002

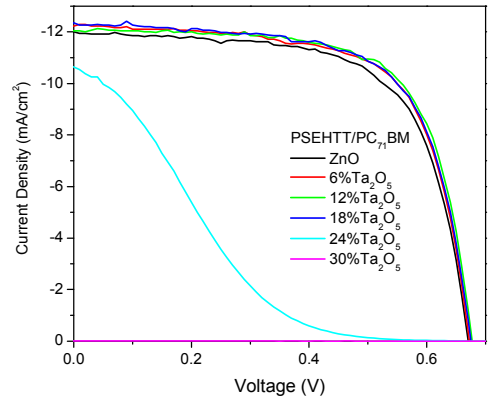

Figure 8. The I–V curve at 1sun and dark condition with various Ta_2O_5-ZnO films as the cathodic buffer layer. (BHJ active layer: PSEHTT:$PC_{71}BM$)

PSEHTT/$PC_{71}BM$ as BHJ active layer and long-term stability

In order to demonstrate the effect of Ta_2O_5-ZnO CBLs for the inverted OPVs with different BHJ systems, PSEHTT/$PC_{71}BM$ was applied as the active layer and replaced the commonly used P3HT/$PC_{61}BM$. PSEHTT is a kind of thiazolothiazole-dithienosilole copolymer semiconductors presented by Jenekhe's group in 2011, and it achieved 5% power conversion efficiency in conventional structure OPVs at that time.[56] Combing PSEHTT/$PC_{71}BM$ and Ta_2O_5-ZnO CBLs to make the inverted structure OPVs, the power conversion efficiency and I-V curves are summarized in **Table 4** and **Figure 8**. The highest efficiency is around 5.6% with 12% Ta_2O_5 film as CBLs, and it is 6% improvement compared with 5.2% efficiency for pure ZnO as CBLs, which means that the Ta_2O_5-ZnO films as CBLs also work for PSEHTT/$PC_{71}BM$ systems to improve the overall power conversion efficiency. It should also be noted that the trend shown in **Figure 8** appears very similar to that in **Figure 2**: when a small amount of Ta_2O_5 was added, the power conversion efficiency increased with the concentration of Ta_2O_5 added and then there was a drastic drop of PCE when Ta_2O_5 content reached a certain level. Therefore, the effect of Ta_2O_5 in CBLs to overall PCE could be taken as similar phenomenon in various kinds for inverted OPVs.

Furthermore, the power conversion efficiency of the unencapsulated inverted OPVs was periodically measured for 42 days to monitor their long-term stability in air (**Figure 9**). All devices retain around 100% of the magnitude of their original power conversion efficiency values after being exposed to ambient conditions for 42 days. This explicitly demonstrates the superior air stability of inverted OPVs.

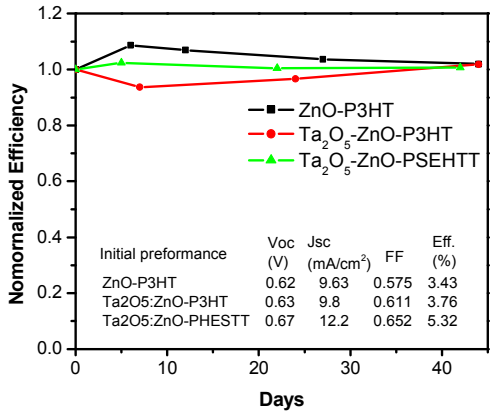

Figure 9. The long term stability of inverted OPVs with ZnO or Ta_2O_5-ZnO films as the cathodic buffer layer; the devices were stored in ambient environment.

Conclusions

Ta_2O_5-ZnO films have been fabricated and demonstrated as the cathodic buffer layers in inverted polymer solar cells for an improved power conversion efficiency. The device performance was found to be strongly dependent on the amount of Ta_2O_5 in CBLs. The data suggested that with Ta exist in CBLs, the Ta-O-Zn bonding was formed, and which is benefit to overall PCE. Moreover, some surface gain boundaries might be covered by Ta_2O_5 and resulted in less oxygen adsorbing site, and also Ta_2O_5, famous for its high

dielectric constant, might provide a self-built electric field on the interface between HBJ active layer and CBL to reduce the electron recombination resulting in enhanced power conversion efficiency. But, a continued increase in the amount of Ta_2O_5 in ZnO film led to lower electron mobility and low crystallinity of CBLs. In the present study, it was found that the power conversion efficiency with P3HT/PC_{61}BM system increases from 3.7% to 4.12%, presenting 11% enhancement, and for PSEHTT/PC_{71}BM system, the power conversion efficiency increases from 5.29% to 5.61%. Moreover, the long-term stability of unencapsulated inverted OPVs was periodically measured for 42 days, and all devices retain around 100% of their original power conversion efficiencies.

Acknowledgements

This work is supported in part by the U.S. Department of Energy, Office of Basic Energy Sciences, Division of Materials Sciences, under Award no. **DE-FG02-07ER46467**.

Notes and references

[a] Department of Material Science and Engineering, University of Washington, Seattle, WA, 98195, USA.
[b] Department of Chemical Engineering, University of Washington, Seattle, WA, 98195, USA.
* e-mail: gzcao@u.washington.edu

1. Po R, Carbonera C, Bernardi A, Camaioni N. The role of buffer layers in polymer solar cells. *Energy Environ Sci*. 2011;4(2):285. doi:10.1039/c0ee00273a.
2. Yu G, Gao J, Hummelen JC, Wudl F, Heeger AJ. Polymer Photovoltaic Cells: Enhanced Efficiencies via a Network of Internal Donor-Acceptor Heterojunctions. *Science (80-)*. 1995;270(5243):1789–1791. doi:10.1126/science.270.5243.1789.
3. Ma W, Yang C, Gong X, Lee K, Heeger AJ. Thermally Stable, Efficient Polymer Solar Cells with Nanoscale Control of the Interpenetrating Network Morphology. *Adv Funct Mater*. 2005;15(10):1617–1622. doi:10.1002/adfm.200500211.
4. Chen H-Y, Hou J, Zhang S, et al. Polymer solar cells with enhanced open-circuit voltage and efficiency. *Nat Photonics*. 2009;3(11):649–653. doi:10.1038/nphoton.2009.192.
5. Ameri T, Dennler G, Lungenschmied C, Brabec CJ. Organic tandem solar cells: A review. *Energy Environ Sci*. 2009;2(4):347. doi:10.1039/b817952b.
6. Liang Y, Xu Z, Xia J, et al. For the bright future-bulk heterojunction polymer solar cells with power conversion efficiency of 7.4%. *Adv Mater*. 2010;22(20):E135–8. doi:10.1002/adma.200903528.
7. Li W, Hendriks KH, Roelofs WSC, Kim Y, Wienk MM, Janssen RAJ. Efficient small bandgap polymer solar cells with high fill factors for 300 nm thick films. *Adv Mater*. 2013;25(23):3182–6. doi:10.1002/adma.201300017.
8. Mühlbacher D, Scharber M, Morana M, et al. High Photovoltaic Performance of a Low-Bandgap Polymer. *Adv Mater*. 2006;18(21):2884–2889. doi:10.1002/adma.200600160.
9. He Y, Chen H-Y, Hou J, Li Y. Indene-C(60) bisadduct: a new acceptor for high-performance polymer solar cells. *J Am Chem Soc*. 2010;132(4):1377–82. doi:10.1021/ja908602j.
10. Li G, Shrotriya V, Huang J, et al. High-efficiency solution processable polymer photovoltaic cells by self-organization of polymer blends. *Nat Mater*. 2005;4(11):864–868. doi:10.1038/nmat1500.
11. Heywang G, Jonas F. Poly(alkylenedioxythiophene)s—new, very stable conducting polymers. *Adv Mater*. 1992;4(2):116–118. doi:10.1002/adma.19920040213.
12. Zhang F, Johansson M, Andersson MR, Hummelen JC, Inganäs O. Polymer Photovoltaic Cells with Conducting Polymer Anodes. *Adv Mater*. 2002;14(9):662–665. doi:10.1002/1521-4095(20020503)14:9<662::AID-ADMA662>3.0.CO;2-N.
13. Yang T, Wang M, Cao Y, et al. Polymer Solar Cells with a Low-Temperature-Annealed Sol-Gel-Derived MoOx Film as a Hole Extraction Layer. *Adv Energy Mater*. 2012;2(5):523–527. doi:10.1002/aenm.201100598.
14. Cheng Y-J, Cao F-Y, Lin W-C, Chen C-H, Hsieh C-H. Self-Assembled and Cross-Linked Fullerene Interlayer on Titanium Oxide for Highly Efficient Inverted Polymer Solar Cells. *Chem Mater*. 2011;23(6):1512–1518. doi:10.1021/cm1032404.
15. Hau SK, Yip H-L, Ma H, Jen AK-Y. High performance ambient processed inverted polymer solar cells through interfacial modification with a fullerene self-assembled monolayer. *Appl Phys Lett*. 2008;93(23):233304. doi:10.1063/1.3028094.
16. You J, Chen C-C, Hong Z, et al. 10.2% power conversion efficiency polymer tandem solar cells consisting of two identical sub-cells. *Adv Mater*. 2013;25(29):3973–8. doi:10.1002/adma.201300964.
17. Kim JS, Friend RH, Cacialli F. Improved operational stability of polyfluorene-based organic light-emitting diodes with plasma-treated indium–tin–oxide anodes. *Appl Phys Lett*. 1999;74(21):3084. doi:10.1063/1.124069.
18. Kawano K, Pacios R, Poplavskyy D, Nelson J, Bradley DDC, Durrant JR. Degradation of organic solar cells due to air exposure. *Sol Energy Mater Sol Cells*. 2006;90(20):3520–3530. doi:10.1016/j.solmat.2006.06.041.
19. De Jong MP, van IJzendoorn LJ, de Voigt MJA. Stability of the interface between indium-tin-oxide and poly(3,4-ethylenedioxythiophene)/poly(styrenesulfonate) in polymer light-emitting diodes. *Appl Phys Lett*. 2000;77(14):2255. doi:10.1063/1.1315344.
20. Hau SK, Yip H-L, Jen AK-Y. A Review on the Development of the Inverted Polymer Solar Cell Architecture. *Polym Rev*. 2010;50(4):474–510. doi:10.1080/15583724.2010.515764.
21. Li G, Chu C-W, Shrotriya V, Huang J, Yang Y. Efficient inverted polymer solar cells. *Appl Phys Lett*. 2006;88(25):253503. doi:10.1063/1.2212270.
22. Zhou Y, Cheun H, Potscavage, Jr WJ, Fuentes-Hernandez C, Kim S-J, Kippelen B. Inverted organic solar cells with ITO electrodes modified with an ultrathin Al2O3 buffer layer deposited by atomic layer deposition. *J Mater Chem*. 2010;20(29):6189. doi:10.1039/c0jm00662a.
23. Liang Z, Zhang Q, Wiranwetchayan O, et al. Effects of the Morphology of a ZnO Buffer Layer on the Photovoltaic Performance of Inverted Polymer Solar Cells. *Adv Funct Mater*. 2012;22(10):2194–2201. doi:10.1002/adfm.201101915.
24. Lee JH, Cho S, Roy A, Jung H-T, Heeger AJ. Enhanced diode characteristics of organic solar cells using titanium suboxide electron transport layer. *Appl Phys Lett*. 2010;96(16):163303. doi:10.1063/1.3409116.
25. Liu J, Choy K-L, Hou X. Charge transport in flexible solar cells based on conjugated polymer and ZnO nanoparticulate thin films. *J Mater Chem*. 2011;21(6):1966. doi:10.1039/c0jm02184a.
26. Hayakawa A, Yoshikawa O, Fujieda T, Uehara K, Yoshikawa S. High performance polythiophene/fullerene bulk-heterojunction solar cell with a TiO[sub x] hole blocking layer. *Appl Phys Lett*. 2007;90(16):163517. doi:10.1063/1.2730746.
27. Kuwabara T, Kawahara Y, Yamaguchi T, Takahashi K. Characterization of inverted-type organic solar cells with a ZnO layer as the electron collection electrode by ac impedance spectroscopy. *ACS Appl Mater Interfaces*. 2009;1(10):2107–10. doi:10.1021/am900446x.
28. Gilot J, Wienk MM, Janssen RAJ. Double and triple junction polymer solar cells processed from solution. *Appl Phys Lett*. 2007;90(14):143512. doi:10.1063/1.2719668.
29. Chen J-Y, Hsu F-C, Sung Y-M, Chen Y-F. Enhanced charge transport in hybrid polymer/ZnO-nanorod solar cells assisted by conductive small molecules. *J Mater Chem*. 2012;22(31):15726. doi:10.1039/c2jm31605f.
30. Chen L-M, Hong Z, Li G, Yang Y. Recent Progress in Polymer Solar Cells: Manipulation of Polymer:Fullerene Morphology and the Formation of Efficient Inverted Polymer Solar Cells. *Adv Mater*. 2009;21(14-15):1434–1449. doi:10.1002/adma.200802854.
31. Hau SK, Cheng Y-J, Yip H-L, Zhang Y, Ma H, Jen AK-Y. Effect of Chemical Modification of Fullerene-Based Self-Assembled

Monolayers on the Performance of Inverted Polymer Solar Cells. *ACS Appl Mater Interfaces*. 2010;2(7):1892–1902. doi:10.1021/am100238e.
32. Shirakawa T, Umeda T, Hashimoto Y, Fujii A, Yoshino K. Effect of ZnO layer on characteristics of conducting polymer/C 60 photovoltaic cell. *J Phys D Appl Phys*. 2004;37(6):847–850. doi:10.1088/0022-3727/37/6/007.
33. Chen C-T, Hsu F-C, Kuan S-W, Chen Y-F. The effect of C60 on the ZnO-nanorod surface in organic–inorganic hybrid photovoltaics. *Sol Energy Mater Sol Cells*. 2011;95(2):740–744. doi:10.1016/j.solmat.2010.10.015.
34. Thitima R, Patcharee C, Takashi S, Susumu Y. Efficient electron transfers in ZnO nanorod arrays with N719 dye for hybrid solar cells. *Solid State Electron*. 2009;53(2):176–180. doi:10.1016/j.sse.2008.10.014.
35. Zhou Y, Fuentes-Hernandez C, Shim J, et al. A universal method to produce low-work function electrodes for organic electronics. *Science*. 2012;336(6079):327–32. doi:10.1126/science.1218829.
36. Bulliard X, Ihn S-G, Yun S, et al. Enhanced Performance in Polymer Solar Cells by Surface Energy Control. *Adv Funct Mater*. 2010;20(24):4381–4387. doi:10.1002/adfm.201000960.
37. Park S, Tark SJ, Lee JS, Lim H, Kim D. Effects of intrinsic ZnO buffer layer based on P3HT/PCBM organic solar cells with Al-doped ZnO electrode. *Sol Energy Mater Sol Cells*. 2009;93(6-7):1020–1023. doi:10.1016/j.solmat.2008.11.033.
38. Kyaw AKK, Sun X, Zhao DW, Tan ST, Divayana Y, Demir HV. Improved Inverted Organic Solar Cells With a Sol–Gel Derived Indium-Doped Zinc Oxide Buffer Layer. *IEEE J Sel Top Quantum Electron*. 2010;16(6):1700–1706. doi:10.1109/JSTQE.2009.2039200.
39. Oo TZ, Devi Chandra R, Yantara N, et al. Zinc Tin Oxide (ZTO) electron transporting buffer layer in inverted organic solar cell. *Org Electron*. 2012;13(5):870–874. doi:10.1016/j.orgel.2012.01.011.
40. Lan J-L, Liang Z, Yang Y-H, Ohuchi FS, Jenekhe SA, Cao G. The effect of SrTiO3:ZnO as cathodic buffer layer for inverted polymer solar cells. *Nano Energy*. 2014;4:140–149. doi:10.1016/j.nanoen.2013.12.010.
41. Thambidurai M, Kim JY, Kang C, et al. Enhanced photovoltaic performance of inverted organic solar cells with In-doped ZnO as an electron extraction layer. *Renew Energy*. 2014;66:433–442. doi:10.1016/j.renene.2013.12.031.
42. Wang ZL. Towards Self-Powered Nanosystems: From Nanogenerators to Nanopiezotronics. *Adv Funct Mater*. 2008;18(22):3553–3567. doi:10.1002/adfm.200800541.
43. Du X, Mei Z, Liu Z, et al. Controlled Growth of High-Quality ZnO-Based Films and Fabrication of Visible-Blind and Solar-Blind Ultra-Violet Detectors. *Adv Mater*. 2009;21(45):4625–4630. doi:10.1002/adma.200901108.
44. Schmidt-Mende L, MacManus-Driscoll JL. ZnO – nanostructures, defects, and devices. *Mater Today*. 2007;10(5):40–48. doi:10.1016/S1369-7021(07)70078-0.
45. Bai Y, Yu H, Li Z, Amal R, Lu GQM, Wang L. In situ growth of a ZnO nanowire network within a TiO(2) nanoparticle film for enhanced dye-sensitized solar cell performance. *Adv Mater*. 2012;24(43):5850–6. doi:10.1002/adma.201201992.
46. Cheun H, Fuentes-Hernandez C, Zhou Y, et al. Electrical and Optical Properties of ZnO Processed by Atomic Layer Deposition in Inverted Polymer Solar Cells †. *J Phys Chem C*. 2010;114(48):20713–20718. doi:10.1021/jp106641j.
47. Noone KM, Subramaniyan S, Zhang Q, Cao G, Jenekhe SA, Ginger DS. Photoinduced Charge Transfer and Polaron Dynamics in Polymer and Hybrid Photovoltaic Thin Films: Organic vs Inorganic Acceptors. *J Phys Chem C*. 2011;115(49):24403–24410. doi:10.1021/jp207514v.
48. Yildirim S, Ulutas K, Deger D, Zayim EO, Turhan I. Dielectric properties of sol–gel derived Ta2O5 thin films. *Vacuum*. 2005;77(3):329–335. doi:10.1016/j.vacuum.2004.12.002.
49. Rubio F, Denis J, Albella JM, Martinez-Duart JM. Sputtered Ta2O5 antireflection coatings for silicon solar cells. *Thin Solid Films*. 1982;90(4):405–408. doi:10.1016/0040-6090(82)90545-4.
50. Ezhilvalavan S, Tseng TY. Preparation and properties of tantalum pentoxide (Ta2O5) thin films for ultra large scale integrated circuits (ULSIs) application – A review. *J Mater Sci Mater Electron*. 1999;10(1):9–31. doi:10.1023/A:1008970922635.
51. Briggs D. Handbook of X-ray Photoelectron Spectroscopy C. D. Wanger, W. M. Riggs, L. E. Davis, J. F. Moulder and G. E.Muilenberg Perkin-Elmer Corp., Physical Electronics Division, Eden Prairie, Minnesota, USA, 1979. 190 pp. $195. *Surf Interface Anal*. 1981;3(4):v–v. doi:10.1002/sia.740030412.
52. Mihailetchi VD, van Duren JKJ, Blom PWM, et al. Electron Transport in a Methanofullerene. *Adv Funct Mater*. 2003;13(1):43–46. doi:10.1002/adfm.200390004.
53. A. J. Moulson JMH. Electroceramics: Materials, Properties, Applications, 2nd Edition. *wiley*. 2003. Available at: http://www.wiley.com/WileyCDA/WileyTitle/productCd-0471497487.html. Accessed March 5, 2014.
54. Wiranwetchayan O. The Role of Oxide Thin Layer in Inverted Structure Polymer Solar Cells. *Mater Sci Appl*. 2011;02(12):1697–1701. doi:10.4236/msa.2011.212226.
55. Verbakel F, Meskers SCJ, Janssen RAJ. Electronic memory effects in diodes from a zinc oxide nanoparticle-polystyrene hybrid material. *Appl Phys Lett*. 2006;89(10):102103. doi:10.1063/1.2345612.
56. Subramaniyan S, Xin H, Kim FS, Shoaee S, Durrant JR, Jenekhe SA. Effects of Side Chains on Thiazolothiazole-Based Copolymer Semiconductors for High Performance Solar Cells. *Adv Energy Mater*. 2011;1(5):854–860. doi:10.1002/aenm.201100215.

